International Journal of Theoretical and Applied Research (IJTAR)

ISSN: 2812-5878

Homepage: https://ijtar.journals.ekb.eg

Original article

Monitoring Spatiotemporal Changes in Land Surface Temperature and Urban Heat Islands of Sharkia Governorate Districts Using Remote Sensing Technology

Alaa Nagy[a*], Ahmed El-Zeiny[b], Mohamed Sowilem[b], Walaa Moselhy[a] and Manal Elshaier[a]

[a] *Department of Zoology and Entomology, Faculty of Science (Girls Branch), Al-Azhar University, Cairo, Egypt.*

[b] *Department of Environmental Studies, National Authority for Remote Sensing and Space Sciences (NARSS), Cairo, Egypt.*

ARTICLE INFO

Received 06/06/2023
Revised 17/10/2023
Accepted 30/11/2023

Keywords

LST
UHI
Remote Sensing
GIS
Landsat
Sharkia Governorate

ABSTRACT

Recent years have experienced rapid urban growth in the Sharkia Governorate. These land demands contribute to a notable variance in Land Surface Temperature (LST), which aggravates the problem of Urban Heat Islands (UHI) caused by climate change. The purpose of this study is to monitor LST and UHI changes in the Sharkia governorate and its districts using remotely sensed data in conjunction with Geographic Information System (GIS) techniques. Three Landsat images acquired in July 2002, 2012, and 2022 were calibrated and processed to map LST changes and identify UHI regions in the past 20 years. Results showed that throughout the whole study period, the governorate experienced persistent spatiotemporal fluctuations in LST ranging from 20.36 to 49.76 °C. The highest mean LST in the whole governorate was recorded during 2022 equaling 38.78 °C. The highest LST increase in districts was reported in Mashtul Elsuq showing a rise in LST by 3.14 °C and in Awlad Saqr by 14.04 °C. UHI showed a continuous increase to reach the maximum area in 2022 (128.14 km^2). However, New Salhia is the only district that had a decline in the UHI areas from 2002 to 2022. The strongest UHI effect is seen in new cities, industrial zones, and metropolitan areas because of anthropogenic heat release. This is confirmed by the significant positive correlation between LST and NDBI (Urban Index). Thus, it was highly recommended that when developing and designing new cities, urban planners and architects should take into account metropolitan areas' thermal characteristics.

Graphical abstract

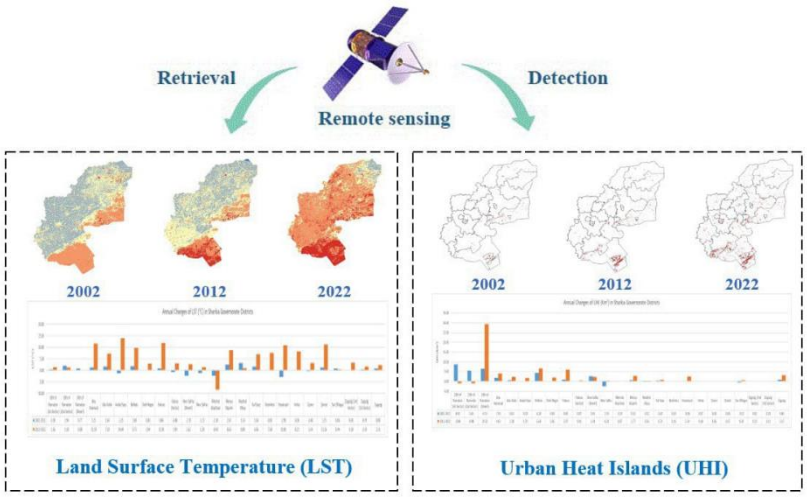

* *Corresponding author*
E-mail address: alaanagy@azhar.edu.eg
DOI: 10.21608/IJTAR.2023.197764.1040

Special issue "selected papers from the 2nd International Conference on Basic and Applied Science (2nd IACBAS-2023)"

1. Introduction

Land surface temperature is one of the most crucial variables in the physical processes of surface energy and water balance at local to global scales. Land Surface

looks through the atmosphere to the ground. Land Surface Temperature estimate provides information on the temporal and geographic fluctuations of the surface equilibrium state and is critically important in many applications [1].

Climate variations in and around cities and other built-up areas are influenced by anthropogenic activity changes. Urban Heat Island is the term used to describe the temperature differential between urban and rural areas. The UHI are areas of anthropogenic climate change that have an impact on the biosphere, the economy, and the atmosphere. The primary source of UHI is the change in land use, although there are other causes as well, such as defining characteristics and human factors. The UHI is also influenced by other factors, including urban sprawl, heat emissions from human heat sources, air pollution, geographic location, and climate [2,3].

Sharkia Governorate is distinguished by a dense population that is surrounded by high structures and industrial facilities and by the lack of open spaces in urban areas. This rapid urban social and economic development may result in serious problems with the urban environment, such as traffic congestion, environmental pollution, and UHI. Among them, UHI is one of the worst environmental issues brought on by changes to the urban landscape [4].

Numerous studies have used land-based observation stations to measure air temperature and determine the relative warmth of urban areas. Some investigations employed temperature sensors installed on cars traveling various routes to monitor temperatures. This approach may be costly, time-consuming, and problematic in terms of spatial interpolation. The aforementioned methods might be improved by remote sensing [4,5]. Conventional UHI studies employing observed temperature data from stationary or mobile monitoring stations may result in a potential bias that may not accurately reflect the overall urban thermal environment [6].

Fortunately, remote sensing is frequently used to track dynamics and changes in land and air observation, as well as their effects on the environment. It has several advantages in LST and UHIs research. Remote sensing is also used to examine historical LST and UHIs and provide data in inaccessible areas. To provide more efficiency, remote sensing is often integrated with GIS techniques. By combining current remotely sensed data with relevant environments, these technologies provide the potential to obtain information on land characteristics and change [7].

Roa [8] was the first to suggest that remote sensing is useful for examining the UHI and constructing a graph showing the thermal gradient of the land surface using the thermal infrared data from satellite images. After that, numerous studies frequently employed satellite images to detect and monitor LST and UHI [3, 6, and 9 - 11]. Therefore, the current study combines remotely sensed data from the Landsat satellites with GIS techniques to evaluate and map LST and UHI in Sharkia Governorate. It contributes to assessing and mapping LST and UHI changes in the past 20 years.

Temperature can be defined more broadly as the hotness of the earth's surface. From the perspective of an RS satellite, the surface is everything that can be seen when it looks through the atmosphere to the ground. Land Surface Temperature estimate provides information on the temporal and geographic fluctuations of the surface equilibrium state and is critically important in many applications [1].

2. Materials and Methods

2.1 Study Area

Sharkia Governorate is one of the East Delta governorates and is situated in Egypt's Eastern Nile Delta. It extends between latitudes 29º 54` and 31º 12` N and longitudes 31º20` and 32º 15` E (Figure 1). Sharkia Governorate is bordered to the north by Manzala Lake and Dakahlia Governorate, and to the west by Qalubia Governorate. Ismailia and Port Said are two Suez Canal Governorates that are located to the east of the Governorate. Because of its location in the Nile Delta in the middle of a fertile district, Sharkia is a center of the cotton and grain trade in Egypt. The governorate extends over 457586 acres. In terms of topography, the region is elevated at a height of around 13 m above mean sea level (a.m.s.l.). The main source of water for Sharkia Governorate is the Damietta branch of the Nile, which is located at the governorate's western border. The governorate is surrounded by several significant irrigation canals, including the Manayef Canal in the north, the Bahr Moyes and Bahr Faqous in the middle, and the Ismailia Canal in the south. Also, the governorate is traversed by significant agricultural drains such as the Mahsama and Bahr El Baqar Drains [12]. Sharkia Governorate consists of 25 districts, their geographic locations and the area are shown in Figure (2). The largest district is 10th of Ramadan (Desert) with a total area of 578.06 km^2, however, the smallest one is Zagazig, (1st Sector) with a total area of 4.95 km^2.

2.2 Landsat Data Acquisition and Analyses

Landsat Imagery Acquisition and Preparation

In this study, three satellite images were acquired from Landsat-7 with Enhanced Thematic Mapper Plus (ETM+) and Landsat-8 with Operational Land Imager and Thermal Infrared Sensor (OLI/TIRS) (path 176, row 039) in July 2002, 2012, and 2022. To distinguish between the various land cover types of spectral fingerprints, summer photos were selected. Sensor-target-illumination geometry, air absorption and scattering, sensor calibration, and satellite data processing techniques, which tend to change over time, are just a few of the variables that have an impact on spectral data collected by satellite sensors. It is required to do a radiometric correction to monitor actual landscape changes as shown by fluctuations in surface reflectance from multitemporal satellite imageries. During image processing, a series of methods known as "radiometric calibration" is employed to adjust for topography, sun angle, distant sensor sensitivity, and atmospheric scattering/absorption. Landsat data were calibrated primarily using radiometric and atmospheric corrections (Table 1) [13].

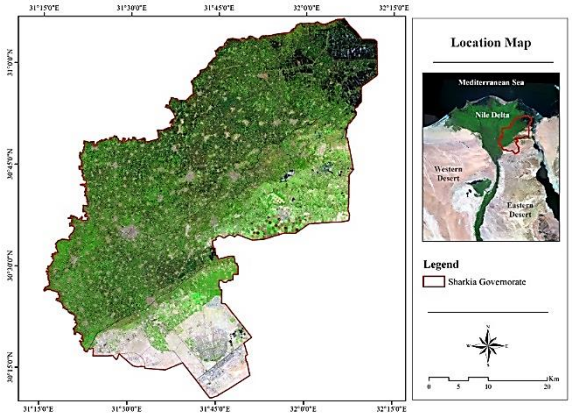

Figure (1). The location map of the study area.

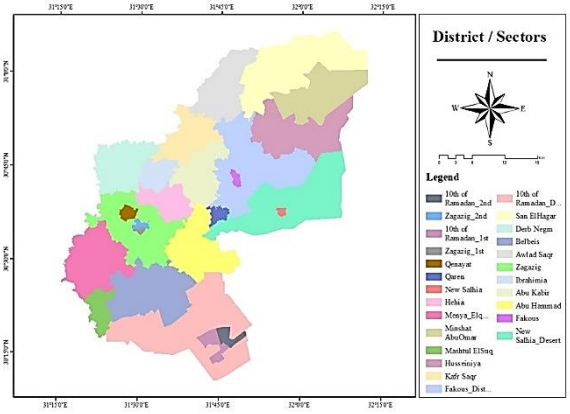

Figure (2). Geographic location of Sharkia Districts

Retrieving land surface temperature

The temperature data acquired by the Landsat sensors is stored as a digital number (DN) having a value between 0 and 255. There is a two-step procedure that can be used to convert these DNs to degrees Kelvin. The DNs are first converted to radiance values using the bias and gain values unique to each scene, and then the radiance data from step one is converted to degrees Kelvin in the following phase [14, 15].

i. Conversion of a digital number to spectral radiance

At sensor radiance L_λ, the digital numbers (DNs) were transformed into tangible measures. Initially, Eq. (1) was used to transform DNs to radiance for Landsat-7, and Eq. (2) for Landsat-8.

$$L_\lambda = \frac{L_{max\lambda} - L_{min\lambda}}{QCal_{max} - QCal_{min}} \text{ x } (Qcal - QCal_{min}) + L_{min\lambda} \quad (1)$$

Where,

- L_λ represents sensor radiance,
- $L_{max\lambda}$ is maximum radiance of band 6,
- $L_{min\lambda}$ is minimum radiance of band 6,
- Qcal is quantized calibrated pixel value in DN,
- $QCal_{max}$ is the maximum quantized calibrated pixel value in DN, and
- $QCal_{min}$ is the minimum quantized calibrated pixel value in DN.

$$L_\lambda = M_L \text{ x } Qcal + A_L \quad (2)$$

Where,

- M_L represents the band-specific multiplicative rescaling factor,
- Qcal is the band 10 image,
- A_L is the band-specific additive rescaling factor, and
- O_i is the correction for band 10.

Table (1). Spectral and technical specifications of Landsat-7 and Landsat-8 satellites.

Satellite	Sensor	Bands	Wavelength (μm)	Spatial Resolution (m)
Landsat- 7	Enhanced Thematic Mapper Plus (ETM+)	Band 1– Blue	0.44 – 0.51	30
		Band 2 – Green	0.52 – 0.6	
		Band 3 – Red	0.63 – 0.69	
		Band 4 – NIR	0.77 – 0.9	
		Band 5 – SWIR 1	1.55 – 1.75	
		Band 6 – TIR	10.31 – 13.36	60
		Band 7 – SWIR 2	2.06 – 2.35	30
		Band 8 – Pan	0.52 – 0.90	15
Landsat- 8	Operational Land Imager and Thermal Infrared Sensor (OLI/TIRS)	Band 1 – Coastal aerosol	0.43 – 0.45	30
		Band 2 – Blue	0.45 – 0.51	
		Band 3 – Green	0.53 – 0.59	
		Band 4 – Red	0.64 – 0.67	
		Band 5 –NIR	0.85 – 0.88	
		Band 6 – SWIR 1	1.57 – 1.65	
		Band 7 – SWIR 2	2.11 – 2.29	
		Band 8 – Panchromatic	0.50 – 0.68	15
		Band 9 – Cirrus	1.36 – 1.38	30
		Band 10 – TIRS1	10.60 – 11.19	100
		Band 11 –TIRS2	11.50– 12.51	

ii. Conversion of radiance values to at-sensor brightness temperature:

The spectral radiance was transformed into at-sensor brightness temperature using Eq. (3);

$$T_B = \frac{K_2}{\ln\left(\left(\frac{K_1}{L_\lambda}\right)+1\right)} \quad (3)$$

Where; Where;

- T_B is the brightness temperature in Kelvin (K),
- L_λ is the spectral radiance in $Wm^{-2}sr^{-1}$
- K_1 and K_2 are the prelaunch calibration constants:

For Landsat-7 K_1= 666.09, and K_2= 1282.71
For Landsat-8 K_1= 774.8853, and K_2= 1321.0789

iii. Estimation of the Land Surface Emissivity from Normalized Difference Vegetation Index

The brightness temperatures acquired above must be adjusted using the emissivity of surface materials to obtain the land surface temperatures. The range of emissivity applied to urban surfaces has been 0.87 to 0.97, with the majority of readings falling between 0.92-0.95. The emissivity is retrieved using El-Zeiny and Effat [14] and Alsultan [16].

iv. Land Surface Temperature Retrieving

After obtaining the emissivity images, the LST can be determined using Eq. (4):

$$LST = \frac{T_B}{1+\left(\frac{\lambda\sigma T_B}{hc}\right)ln\varepsilon} - 273.15 \quad (4)$$

Where λ is the effective wavelength (10.895 µm for band 10 TM+), σ is Boltzmann constant (1.38 x 10^{-23} J/K), h is Plank's constant (6.626 x 10^{-34}Js), c is the velocity of light at a vacuum (2.998 x 10^{-8} m/sc), ε is emissivity [14]. Temperatures were classified into appropriate ranges and color-coded to generate a thermal pattern distribution map of LST over the study area.

v. Urban Heat Island Mapping

The difference between the average temperature of the urban area and that of the rural area is used to determine the intensity of UHI [17].

LST> μ+0.5× δ referred to the UHI area.

Where μ and δ are the mean and standard deviation of temperatures in the study area, respectively.

Data analysis

The spatial distribution of LST and UHI was mapped using ArcMap 10.5 software. Data Analysis toolbox from the Excel computerized program was used for statistical analysis. Minimum, maximum, mean, and standard deviation were calculated for LST

3. Results and Discussion

Assessing Land Surface Temperature in Sharkia Governorate

Statistics of LST in Sharkia Governorate over 2002, 2012, and 2022 are illustrated in Table (2). It was noticed that the high LST was recorded in 2022, ranging between 20.36 – 49.76 °C with a mean of 38.78 °C (SD= 2.24). Figure (5) shows LST spatial variations over the governorate. It was found that the high LST was compatible not only with the urbanized area but rather it was increased over the desert (bare land) areas. This is attributed to the lack of water bodies and vegetation in the desert. These findings agree with El-Zeiny and Effat [14], who reported that LST was elevated in the urbanized and bare-lands areas than in the agricultural lands and water bodies.

By assessing the LST in Sharkia Districts, it was found major fluctuations in LST during the whole period of study. Most districts recorded a continuous increase in LST from 2002 to 2022. This was shown in 10th of Ramadan (1st Sector), 10th of Ramadan (2nd Sector), 10th of Ramadan (Desert), Abu Hammad, Abu Kabir, Belbeis, Fakous, Menya Elqamh, Mashtul Elsuq, Kaf Saqr, Qeniat, San Elhagar, Zagazig (1st Sector), and Zagazig. On the other hand, Derb Negm, Ibrahimia, Hehia, and Zagazig (2nd Sector) showed the same LST in 2002 and 2012, then increased in 2022, respectively. However, LST followed the order of 2012 < 2002 < 2022 in Awlad Saqr, Fakous (Sector), New Salhia (Desert), New Salhia, Minshat AbuOmar, and El-Husseiniya as shown in Table (3). These fluctuations could be mainly due to human activities, urban development and sprawl, and land reclamation in addition to desertification and degradation occurring in each district.

Table (2). Statistics of Land Surface Temperature and Urban Heat Islands in Sharkia Governorate over 2002, 2012, and 2022.

Year	LST (°C)				UHIs (°C)	UHIs (km^2)
	Min	Max	Mean	SD		
2002	27.93	45.56	36.66	2.08	> 37.7	31.01
2012	21.41	45.56	35.61	3.62	> 37.42	64.71
2022	20.36	49.76	38.78	2.24	> 39.9	128.14

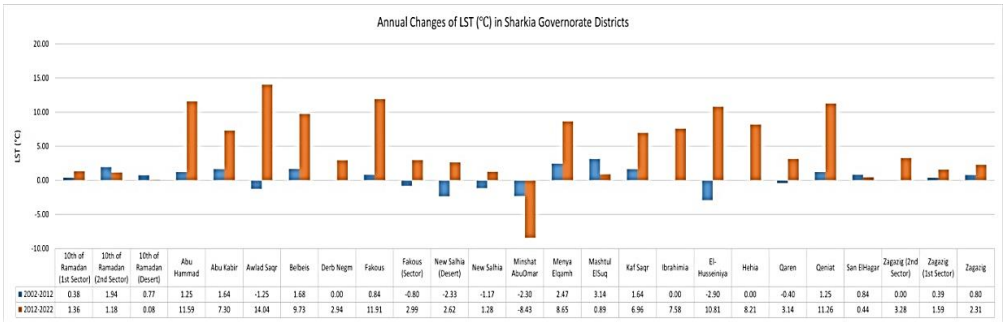

Figure (3). Annual rate of decrease/increase in Land Surface Temperature (°C) during the periods of study.

Table (3). Land Surface Temperature and Urban Heat Islands Averages in Sharkia Districts over 2002, 2012, and 2022.

Districts	LST (°C)			UHI (km^2)		
	2002	2012	2022	2002	2012	2022
10th of Ramadan (1st Sector)	39.16	39.55	40.90	4.22	13.03	12.05
10th of Ramadan (2nd Sector)	36.83	38.78	39.96	3.21	8.67	7.69
10th of Ramadan (Desert)	38.39	39.16	39.25	4.68	11.21	40.53
Abu Hammad	27.93	29.18	40.78	0.48	2.41	6.43
Abu Kabir	29.60	31.24	38.54	0.13	0.76	3.14
Awlad Saqr	28.77	27.52	41.55	0.38	0.35	2.05
Belbeis	26.25	27.93	37.66	1.71	5.99	12.67
Derb Negm	35.65	35.65	38.59	0.01	0.01	2.07
Fakous	27.10	27.93	39.85	0.97	1.82	7.79
Fakous (Sector)	34.46	33.66	36.66	0.01	0.08	0.50
New Salhia (Desert)	39.16	36.83	39.45	9.27	11.92	14.20
New Salhia	38.39	37.22	38.50	3.21	0.68	0.48
Minshat AbuOmar	40.69	38.39	29.96	0.94	0.81	0.88
Menya Elqamh	28.77	31.24	39.89	0.62	1.15	3.92
Mashtul Elsuq	34.86	38.00	38.89	0.01	0.33	0.69
Kaf Saqr	30.01	31.65	38.61	0.07	0.50	1.21
Ibrahimia	28.77	28.77	36.35	0.00	0.03	0.19
El-Husseiniya	30.83	27.93	38.75	1.40	1.34	3.88
Hehia	28.35	28.35	36.56	0.01	0.07	0.25
Qaren	32.86	32.46	35.59	0.00	0.00	0.06
Qeniat	27.93	29.18	40.45	0.00	0.00	0.15
San Elhagar	27.10	27.93	28.37	2.34	1.82	2.41
Zagazig (2nd Sector)	33.66	33.66	36.94	0.00	0.02	0.15
Zagazig (1st Sector)	36.83	37.22	38.81	0.09	0.29	0.40
Zagazig	33.26	34.06	36.37	0.24	1.04	4.21

In order to analyze the changes that occurred in each period separately, the annual change in LST was also determined (Figure 3). Slight variations were noticed during the period of 2002-2012. The maximum increase of LST reached 3.14 °C in Mashtul Elsuq, while the maximum decrease was recorded in El-Husseiniya equaling -2.9 °C. Contrarily, the period of 2012-2022 experienced major increases in LST in most districts with a maximum increase of 14.04 °C recorded in Awlad Saqr. However, Minshat AbuOmar was the only district during this period with a decline in LST, reaching - 8.43 °C. This can be attributed to the district's developmental activities (such as urban development and desert reclamation), which significantly impacted land cover and, in turn, LST throughout this time. In addition, the relation of LST, NDVI, and NDBI was assessed by the correlation coefficient. It was found that the correlation between LST-NDVI and LST-NDBI were -0.77 and 0.88. This demonstrated that there is a substantial relation between NDBI and LST and an inverse correlation between NDVI and LST. Consistent with these findings, Mallick *et.al.* [2] and Sajib and Wang [18] revealed that there is

a strong negative correlation between LST and agricultural areas.

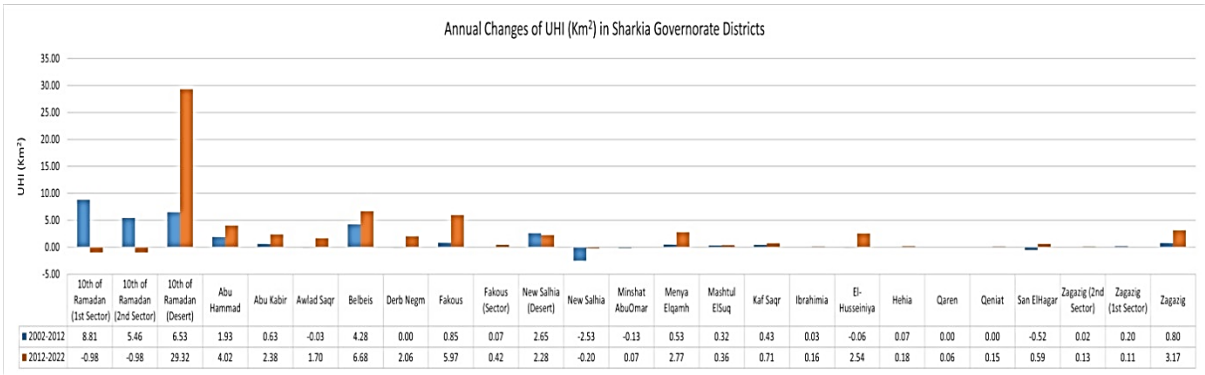

	10th of Ramadan (1st Sector)	10th of Ramadan (2nd Sector)	10th of Ramadan (Desert)	Abu Hammad	Abu Kabir	Awlad Saqr	Belbeis	Derb Negm	Fakous	Fakous (Sector)	New Salhia (Desert)	New Salhia	Minshat AbuOmar	Menya Elqamh	Mashtul ElSuq	Kaf Saqr	Ibrahimia	El-Husseiniya	Hehia	Qaren	Qeniat	San ElHagar	Zagazig (2nd Sector)	Zagazig (1st Sector)	Zagazig
2002-2012	8.81	5.46	6.53	1.93	0.63	-0.03	4.28	0.00	0.85	0.07	2.65	-2.53	-0.13	0.53	0.32	0.43	0.03	-0.06	0.07	0.00	0.00	-0.52	0.02	0.20	0.80
2012-2022	-0.98	-0.98	29.32	4.02	2.38	1.70	6.68	2.06	5.97	0.42	2.28	-0.20	0.07	2.77	0.36	0.71	0.16	2.54	0.18	0.06	0.15	0.59	0.13	0.11	3.17

Figure (4). Annual rate of decrease/increase in Urban Heat Islands (km^2) during the periods of study.

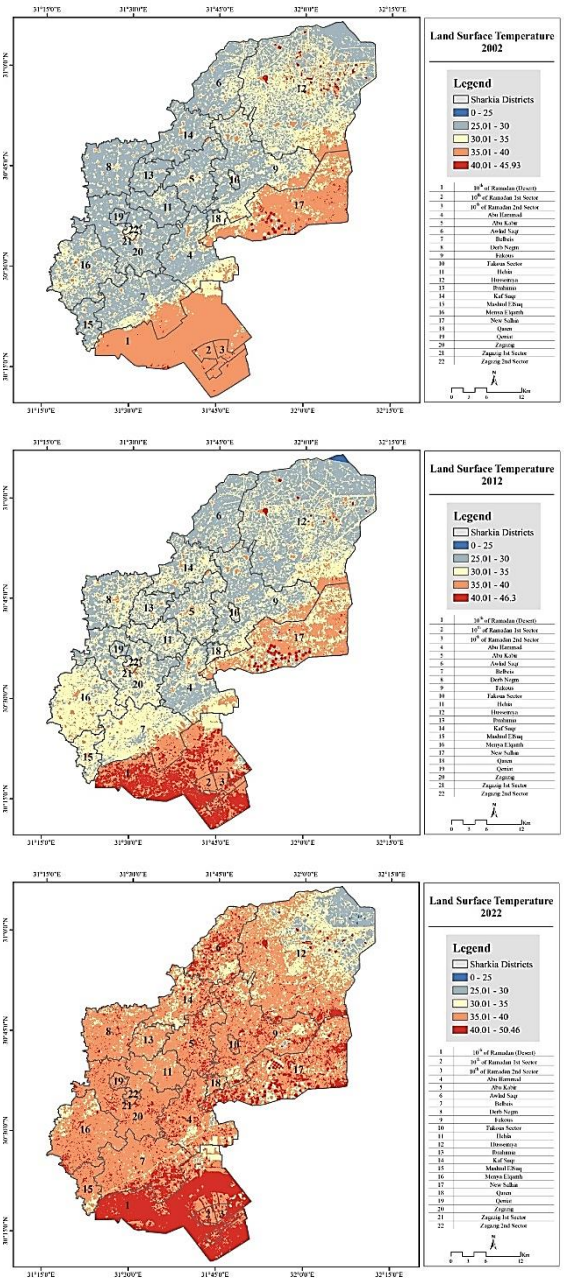

Figure (5). Spatial distribution maps for Land Surface Temperature in Sharkia Governorate over 2002, 2012, and 2022.

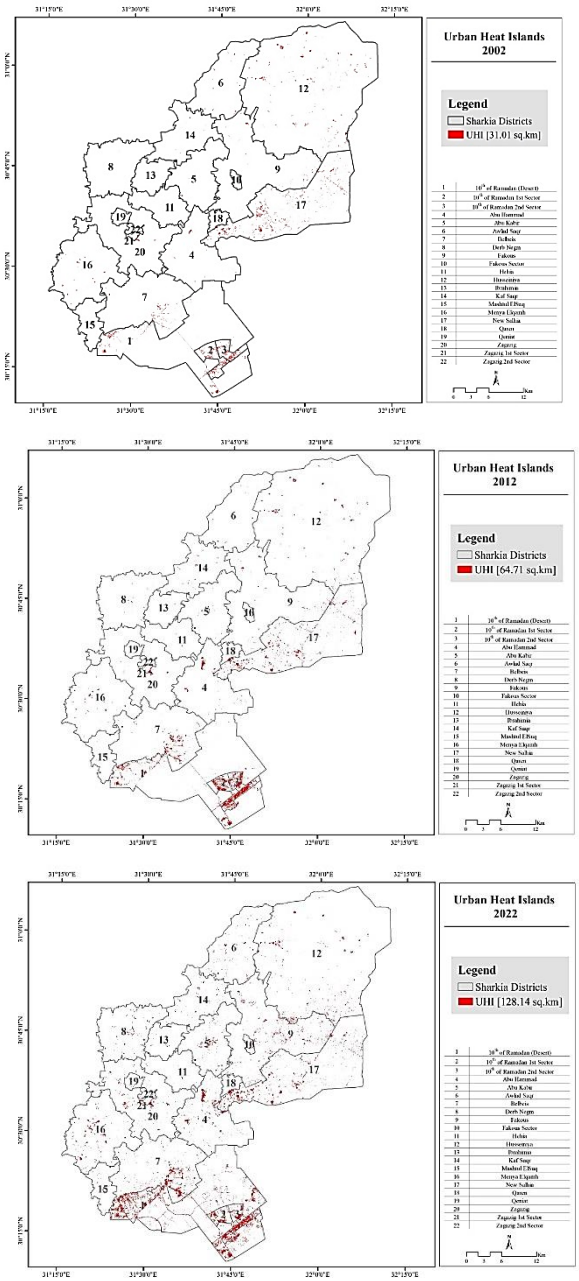

Figure (6). Spatial distribution maps for Urban Heat Islands in Sharkia Governorate over 2002, 2012 and 2022.

Identifying Urban Heat Island in Sharkia Governorate

Statistics and spatial distribution of UHIs are illustrated in Table (2) and Figures (4 & 6). It was noticed that UHI areas continuously increased from 2002 to 2022 reaching a total area of 128.14 km^2 in 2022. Figure (6) showed that the spatial pattern of the UHI regions changed from a pattern, in which bare-land and urban areas were warmer than other areas, in 2002, and 2012 to a more contiguous pattern of UHI in 2022, in conjunction with the expansion of the urban areas. The obtained results showed that the increase of UHI area in the second period (2012-2022), equaling 33.7 km^2, was more than the first period (2002-2012), reaching 81.43 km^2, as a result of the increased rate of urbanization. The strongest UHI effect was seen in new cities, industrial zones, and metropolitan areas because of anthropogenic heat release from air conditioners, vehicles, and other artificial heat sources as well as air pollution. These findings were in line with previous studies [3, 19] that map UHI and assess the associated environmental characteristics in Cairo and Qalyubia Governorate, respectively. Moreover, UHI areas were evaluated and determined in all districts as shown in Table (3). Most of the districts followed the order of 2002 < 2012 < 2022 in UHI increase. However, Awlad Saqr, Minshat AbuOmar, El-Husseiniya, and San Elhagar had a slight decrease from 2002 to 2012, which was followed by an increase in 2022. Moreover, it was clearly found that the UHI in New Salhia decreased from 2002 to 2022. This could be due to land reclamation and an increase in vegetation canopy that declines UHI effects, as stated in a study conducted by Susca *et al.* [20].

4. Conclusion

Due to the negative effects of UHI on human health, energy consumption, and environmental components, evaluating the patterns of these phenomenon's distribution might significantly contribute to minimizing its consequences. In the current study, thermal data from Landsat was integrated with GIS to evaluate and monitor LST and UHI of Sharkia Governorate in the past 20 years. It was found that Sharkia Governorate displayed noticeable variations in LST over the entire study period. Areas with maximum LST existed in the bare lands and were limited to the eastern and southern parts. From 2002 through 2012, Mashtul Elsuq recorded the maximum increase of LST reached 3.14 °C, while the maximum increase of LST during the second period was found in Awlad Saqr with a total degree of 14.04 °C. The LST investigations revealed that anthropogenic activities had an impact on the thermal properties of the environment. By assessing the UHI in the governorate, it was found that these regions continuously increased during the period of the study (2002-2022) reaching a total area of 128.14 km^2. Majority of Sharkia districts followed the order of 2002 < 2012 < 2022 in UHI changes. However, New Salhia had an obvious decrease from 2002 to 2022. The UHIs are typically associated with places where there are residential areas close to industrial zones and bare fields. Therefore, it is highly recommended that when creating and designing cities, urban planners, designers, and architects take into account the thermal characteristics of metropolitan areas.

5. Acknowledgment

Appreciation to the United States Geological Survey (USGS), National Aeronautics and Space Administration (NASA), and Sentinel Hub for supporting satellite images in this research and to the National Authority for Remote Sensing and Space Sciences (NARSS) for support and help.

References

1. W. Kustas, M. Anderson, *Advances in thermal infrared remote sensing for land surface modeling*. Agricultural and Forest Meteorology 149(2009) 2071–2081. doi: 10.1016/j.agrformet.2009.05.016.
2. J. Mallick, Y. Kant, B. Bharath, *Estimation of Land Surface Temperature over Delhi Using Landsat-7 ETM+*. The Journal of Indian Geophysical Union 12(2008) 131-140. http://www.igu.in/12-3/5javed.pdf.
3. M. Ibrahim, M. El-Gammal, A. Shalaby, A. El-Zeiny, N. Rostom, *Environmental and Spatial Assessment of Urban Heat Islands in Qalyubia Governorate, Egypt.* Egyptian Journal of Soil Science, 59(2) (2019) 157-174. doi: 10.21608/ejss.2019.10917.1258.
4. A. Fahmy, M. Abdelfatah, G. El-Fiky, *Investigating land use land cover changes and their effects on land surface temperature and urban heat islands in Sharqiyah Governorate, Egypt.* The Egyptian Journal of Remote Sensing and Space Science. 26(2) (2023) 293-306. doi: 10.1016/j.ejrs.2023.04.001.
5. G. Kaplan, U. Avdan, Z. Avdan, *Urban Heat Island Analysis Using the Landsat 8 Satellite Data: A Case Study in Skopje, Macedonia*. Proceedings 2(2018) 358. doi: 10.3390/ecrs-2-05171.
6. L. Xiong, S. Li, B. Zou, F. Peng, X. Fang, Y. Xue, *Long Time-Series Urban Heat Island Monitoring and Driving Factors Analysis Using Remote Sensing and Geodetector*. Frontiers in Environmental Science 9(2022) 828230. doi: 10.3389/fenvs.2021.828230
7. D. Williams, S. Goward, T. Arvidson, *Landsat: yesterday, today, and tomorrow.* American Society for Photogrammetric Engineering & Remote Sensing 72 (10) (2006) 1171. doi: 10.14358/PERS.72.10.1171.
8. P. Rao, *Remote sensing of urban heat islands from an environmental satellite.* The Bulletin of the American Meteorological Society 53 (1972) 647-648.
9. Q. Weng, *Thermal infrared remote sensing for urban climate and environmental studies: methods, applications, and trends.* The ISPRS Journal of Photogrammetry and Remote Sensing 64 (2009) 335–344. doi: 10.1016/j.isprsjprs.2009.03.007.

10. A. Buyantuyev, J. Wu, *Urban Heat Islands and Landscape Heterogeneity: Linking Spatiotemporal Variations in Surface Temperatures to Land-Cover and Socioeconomic Patterns.* Landscape Ecology 25 (1) (2010) 17–33. doi: 10.1007/s10980-009-9402-4
11. M. Amorim, V. Dubreuil, *Intensity of Urban Heat Islands in Tropical and Temperate Climates.* Climate 5 (2017) 91. doi: 10.3390/cli5040091.
12. ESIAF, *Delta Governorates – Executive summary. Institute of environmental studies and research. Framework for the Environmental and Social Impact Assessment Framework (ESIAF).* ISSIP 2- Project. Ain Shams University, Egypt, 2010.
13. A. El-Zeiny, S. El-Kafrawy, *Assessment of water pollution induced by human activities in Burullus Lake using Landsat 8 operational land imager and GIS.* The Egyptian Journal of Remote Sensing and Space Science 20 (2017) S49–S56.
14. A. El-Zeiny, H. Effat. *Environmental monitoring of spatiotemporal change in land use/land cover and its impact on land surface temperature in El-Fayoum governorate, Egypt*. Remote Sensing Applications: Society and Environment 8(2017) 266-277.https://doi.org/10.1016/j.rsase.2017.10.003.
15. J. Sobrino, J. Jimenez-Munoz, L. Paolini, *Land surface temperature retrieval from Landsat TM5.* Remote Sensing of Environment 9 (2004) 434–440. https://doi.org/10.1016/j.rse.2004.02.003.
16. S. Alsultan, H. Lim, M. Matjafri, K. Abdullah. *An algorithm for land surface temperature analysis of remote sensing image coverage over Al Qassim, Saudi Arabia*. Remote Sensing and Photogrammetry (27) (2005).
17. H. Effat, O. Hassan. *Change detection of urban heat islands and some related parameters using multi-temporal Landsat images; a case study for Cairo city, Egypt*. Urban Climate 10 (2014) 171–188. https://doi.org/10.1016/j.uclim.2014.10.011.
18. M. Sajib, T. Wang, *Estimation of Land Surface Temperature in an Agricultural Region of Bangladesh from Landsat 8: Intercomparison of Four Algorithms*. Sensors. 20(6) (2020) 1778. https://doi.org/10.3390/s20061778.
19. M. El-Hattab, S. Amany, G. Lamia. *Monitoring and assessment of urban heat islands over the Southern region of Cairo Governorate, Egypt.* The Egyptian Journal of Remote Sensing and Space Science. 21 (3) (2018) 311-323. https://doi.org/10.1016/j.ejrs.2017.08.008.
20. T. Susca, S. Gaffin, G. Dell. *Positive effects of vegetation: urban heat island and green roofs.* Environmental Pollution 159(8-9) (2011) 2119–2126. https://doi.org/10.1016/j.envpol.2011.03.007.